Journal Name

COMMUNICATION

One-Pot Polyol Synthesis of Highly Monodisperse Short Green Silver Nanorods

Received 00th January 20xx,
Accepted 00th January 20xx

DOI: 10.1039/x0xx00000x

www.rsc.org/

Javier Patarroyo,[a,b] Aziz Genç,[a,c] Jordi Arbiol,[a,e] Neus G. Bastús,[a] and Victor Puntes.[*a,d,e]

Green silver nanorods (Ag NRs) of low aspect ratio (2.8) have been produced in high yields via an optimized, simple, and robust one-pot polyol method in the presence of tannic acid, which favors the nucleation of decahedral seeds needed for the production of monodisperse Ag NRs. These Ag NRs were further used as sacrificial templates to produce Au hollow nanostructures via galvanic replacement reaction with $HAuCl_4$ at room temperature.

Ag nanorods (NRs) are emerging interesting materials with increasing importance from the perspectives of both, fundamental science, and potential plasmonic and electronic applications.[1] Their unique size and shape-dependent physical and chemical properties make them attractive for many technologies including, among other, optical and flexible electronic devices, catalysis, surface enhanced Raman scattering (SERS)-active platforms and biosensing.[1, 2]

The reproducible fabrication of highly monodisperse Ag NRs with controlled sizes is a challenging task. First studies, pioneered by Murphy and co-workers,[3] reported the production of cylindrical Ag NRs in water by the use of cetyltrimetylammonium bromide (CTAB) as shape-directing agent and citrate-stabilized Ag seeds, which opened the possibility of solution phase methods for the growth of anisotropic metal nanostructures. However, the limited control of the exposed Ag crystal facets and the abundant presence of self-nucleating spherical and anisotropic (platelets and prisms) by-products hamper its reproducible synthesis. These restrictions arise from the difficulty in controlling the anisotropic growth of the Ag crystals after the nucleation of the Ag seeds, typically attributed to the lack of control of their crystal structure (a mixture of single crystal and penta-twinned phases).[4] In this regard, the controlled production of Ag seeds with a decahedral structure has been reported as a necessary requirement to break the fcc symmetry and grow Ag anisotropic structures.[9, 11] However this synthetic crystallographic control of the Ag seeds is still difficult to achieve and only few strategies have reported the controlled production of decahedral Ag seeds via complex time-consuming photochemical irradiation methods.[5, 6] leading to the production of Ag NRs with an improved control of their aspect ratios thanks to the effects of irradiation in the crystal structure of the Ag seeds. Alternatively, Ag NRs with a pentagonal cross section have been produced via seeded-growth strategies using well-faceted decahedral seeds of another metal, mainly Au or Pd.[7-12]

The problem of seed crystalline dispersity has been partially overcome when producing long Ag nanowires (Ag NWs) by the solution-phase seeded-growth polyol approach,[13-19] pioneered by Xia and co-workers. Although the extensive research performed in this system,[14, 16, 20] this route is limited to the production of high aspect ratio Ag NWs with relatively large dimeters (> 40 nm) and, more importantly, highly polydisperse lengths up to 50 µm. In this regard, especially interesting is the work of El-Sayed and co-workers[21] who reported the possibility to obtain short Ag NRs of ~20 nm in diameter (and different lengths) by the temporal quenching of the Ag NWs growth process. However this resulted in very low silver conversion rates and reaction yields.

In this context, the relatively large and polydisperse size of standard Ag seeds, the lack of synthetic control of their crystallinity (often a mixture between single crystal and dodecahedral), and the tendency to form abundant by-products in their production, limit the control of the final Ag NR morphology.[5, 6] Additionally, in most preparation procedures there are multiple synthetic steps involved, which entail tedious post-processing protocols, limit the accurate, reproducible and robust production of Ag NR structures. As a result, it remains difficult to synthesize Ag NRs with controlled

[a] *Institut Català de Nanociència i Nanotecnologia (ICN2), Campus UAB, 08193, Bellaterra, Barcelona, Spain. E-mail:victor.puntes@icn.cat*
[b] *Universitat Autònoma de Barcelona (UAB), Campus UAB, 08193, Bellaterra, Barcelona, Spain.*
[c] *Department of Metallurgy and Materials Engineering, Faculty of Engineering, Bartin University, 74100, Bartin, Turkey.*
[d] *Vall d'Hebron Institut de Recerca (VHIR), 08035, Barcelona, Spain.*
[e] *Institució Catalana de Recerca i Estudis Avançats (ICREA), 08010, Barcelona, Spain.*

† Electronic Supplementary Information (ESI) available: [Experimental details, photograph showing the time evolution of the reaction, and HR-TEM images]. See DOI: 10.1039/x0xx00000x

sizes and low aspect ratios in high yields and with fairly monodisperse distributions.

Herein, we take advantage of well-stablished polyol synthesis of Ag nanostructures to report a simple and robust kinetically controlled one-pot method for the synthesis of short Ag NRs in high yields. These short Ag NRs have an exceptional colloidal stability and a high absorbance in the visible range. The controlled formation and growth of Ag NRs with an average length of 55 nm and diameter of 19 nm is achieved by the use of tannic acid (TA) at substoichiometric concentrations as co-reducing agent[22, 23] in the ethylene glycol (EG) reduction of CF_3COOAg in the presence of high molecular weight PVP (MW 1,300,000). As previously reported,[23-25] the use of a co-reducer favors the massive nucleation of monodisperse seeds, which further grow by the incorporation of the remaining precursor in solution, leading to the high yield production of highly monodisperse low aspect ratio (2.8) Ag NRs. These Ag NRs can be further grown or used as sacrificial templates to produce Au hollow nanostructures via galvanic replacement reaction (GRR) with $HAuCl_4$ which reveals their homogeneous crystal structure.

In a typical synthesis of Ag NRs, an EG solution which acts as solvent and reducing agent, containing a specific amount of CF_3COOAg, high molecular weight PVP (MW 1,300,000), and TA is heated to 170°C in a silicon oil bath under magnetic stirring for 20 min (see the ESI† for synthesis details). The solution turns from yellow to orange, red and finally intense green 15 min later (Fig. S1), and then it is cooled down and prepared for analysis. High angle annular dark field scanning transmission electron microscopy (HAADF-STEM) images of the obtained product, shown in Fig. 1A and C, together with transmission electron microscopy (TEM) images, shown in Fig. 1B, demonstrate that the as-obtained product consist on uniform Ag NRs with an average length of 55.6 ± 9.3 nm and diameter of 19.3 ± 3.0 nm. The average aspect ratio of these NRs is 2.8. The image contrast variations within the same Ag NRs observed in Fig. 1D suggest the presence of a multi-twinned structure. This is confirmed in Fig. 1E showing a HR-TEM image of a single Ag NR, in which the presence of twin boundaries is clearly visible. From one of the facets on the edge, it is possible to identify the face centered cubic (f.c.c.) Ag phase. Detail of the red squared region and its corresponding fast Fourier transformation patterns are shown on Fig. 1F and 1G respectively (see also ESI† Fig. S2), indicating that the NR is composed of face centered cubic (f.c.c.) Ag phase with lattice parameter of a = 0.408 nm, and this particular face is visualized along its [011] zone axis.

The UV−Vis spectrum of the Ag NRs is shown in Fig. 1H. Interestingly, this Ag NRs exhibit two strong absorption peaks, located at 410 and 627 nm, which can be assigned to the transverse and longitudinal surface plasmon resonances (SPRs) respectively. The as-prepared colloidal sample appears intense green, as displayed in the Fig. 1I, which is definitely diverse from the color of spherical Ag NPs and Ag NWs.[15, 22] Fig. 1J shows the measured X-ray diffraction (XRD) patterns. Four diffraction peaks were observed, indexed to (111), (200), (220)

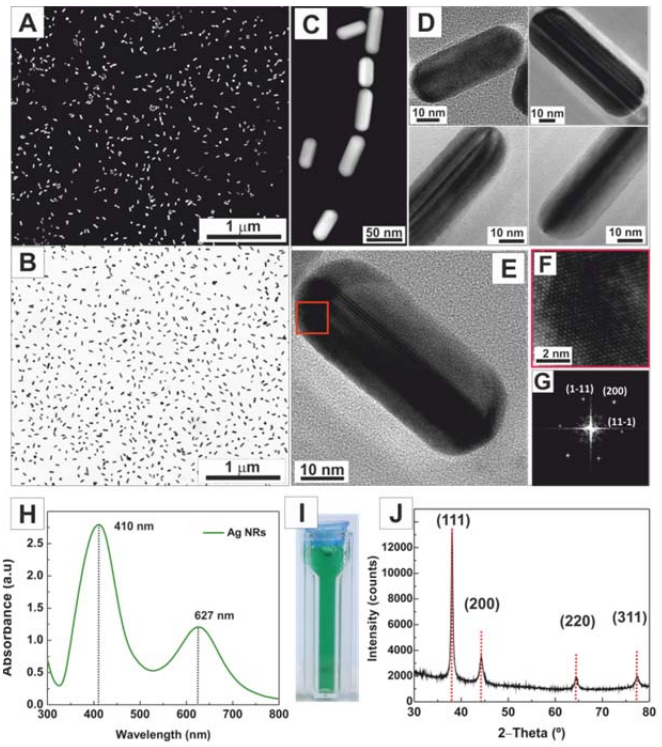

Fig. 1. **A.** Low magnification high-angle annular dark-field scanning TEM (HAADF-STEM) image **B.** Low magnification TEM image **C.** HAADF-STEM image **D.** and **E**. TEM images of Ag NRs. **F.** HRTEM image of the red squared area in E. **G.** Power spectrum of F. **H.** UV–Vis spectrum of the as synthesized Ag NRs **I.** Photograph of aqueous dispersion of Ag NRs. **J.** X-ray diffraction (XRD) patterns of Ag NRs, in red bulk positions and relative intensities of the different diffraction peaks.

and (311) planes, which can be attributed to the fcc structure of Ag (JCPDS file No. 04-0783). The alterations in the XRD peak intensity profile with respect to the standards (the 111 peak is enhanced), and the differences in the peak width measured at medium height (the 111 peak is narrower), accounts for the growth of the rods in the (111) crystal direction.

The key factors for the formation of Ag NRs in high yields are i) the use of TA as a co-reducing agent, ii) the presence of high molecular weight PVP (MW 1,300,000), iii) relatively high temperatures, and iv) the use of CF_3COOAg as source of Ag^+ ions. In detail, TA at low concentration plays the role to produce the initial rapid reduction of a fraction of the Ag precursor,[22] leading to the production of decahedral seeds (Fig. S3). Once the TA has been exhausted, EG slowly reduces the remaining Ag precursor promoting the uniform growth of the formed seeds, avoiding conditions for new nucleation of NCs and the consequently formation of by-products.[22, 26] In control experiments, the yield of Ag NRs dramatically decreased (down to 10%) by performing the reaction in the absence of TA, leading to the production of a large number of by-products of random shapes (spherical, cubes) and only a small fraction of Ag NRs, which are heterogeneous in length and diameter (Fig. 2A, left). As expected, the effect of TA on the final yield and morphology of Ag NRs is concentration dependent. Thus, when the final concentration of TA was increased from 0.0025mM to 0.025mM (Fig. 2A, centre and right) the amount of by-products decreases, obtaining a

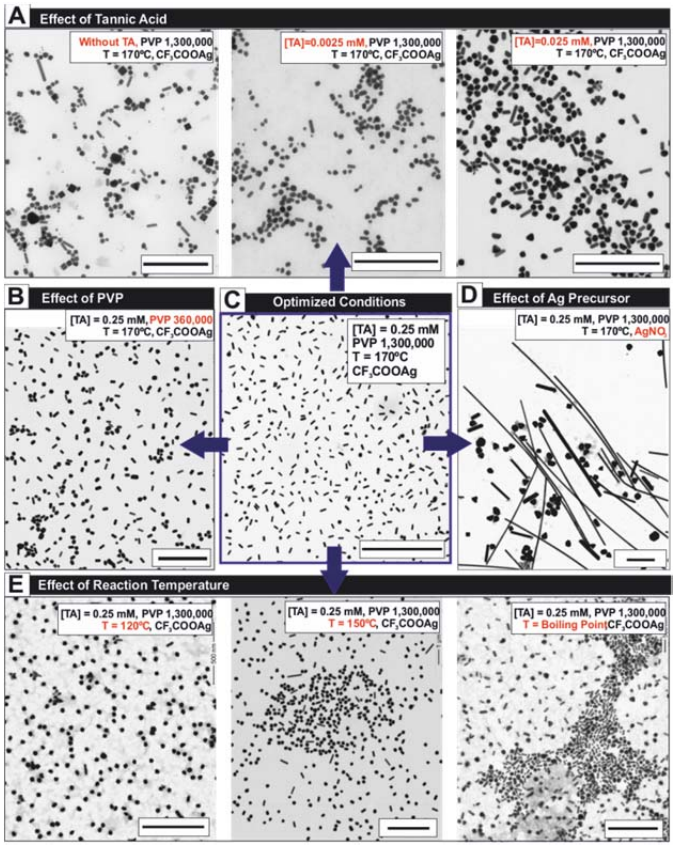

Fig. 2. TEM image of samples obtained upon variation of: A. Concentration of TA. B. PVP chain length. D. Ag precursor. E. Reaction temperature. C. TEM image of samples obtained after optimization of reaction parameters. The scale bar is 500 nm for all images.

sample of Ag NRs with high morphological yield, when the concentration was fixed at 0.25 mM. As previously discussed, the formation of decahedral seeds is necessary for the anisotropic growth of Ag NRs[27] assisted by the presence of high molecular weight PVP. It is well known that high molecular weight PVP binds preferentially on the side of {100} facets of the multiple twined Ag crystal[5, 28-31] leading to the deposition of Ag atoms onto the {111} facets. Besides, variations on the molecular weight of PVP also allow controlling the morphology and yield of the final products. Thus, while the use of PVP with a high molecular weight (MW 1,300,000) favours the formation of uniform Ag NRs, experiments performed using a PVP with a lower molecular weight (MW 360,000) lead to the formation of Ag NRs with a very low aspect ratio, together with a large amount of spherical by-products (Fig. 2B).

Another parameter of control is the reactivity of the Ag precursor. The formation of Ag NRs of low aspect ratio was successfully achieved when using CF_3COOAg as a precursor while the choice of $AgNO_3$, widely used in the standard polyol synthesis, consistently lead to the formation of heterogeneous Ag NWs together with different by-products (Fig. 2D). The argument here accepted is the higher stability of the trifluoroacetate group,[32, 33] since the nitrate group may decompose at elevated temperatures generating ionic and/or gaseous species which can interfere with the NRs formation process.[33]

The morphology of Ag NRs also strongly depends on the reduction rate of Ag^+ ions, which is ultimately determined by the reaction temperature. Thus, running the reaction at 120°C the reducing strength of EG is not enough to drive the growth of Ag NRs, resulting in a final spherical product (Fig. 2E, left), whereas the increase in the temperature to 170°C increases the abundance of Ag NRs (Fig. 2E, center). When the reaction is carried at reflux (197°C), the number of byproducts increases dramatically (Fig. 2E, right). Taken together, we found that the best results were obtained at 170°C, with PVP of high molecular weight (1,300,000), using CF_3COOAg as silver precursor, in the presence of TA at 0.25 mM (Fig. 2C).

The produced Ag NRs can be transformed at room temperature into noble-metal AgAu hollow NRs, via GRR.[34, 35] These reactions, sensitive to the chemical (oxidation state) and the physical (accessibility) nature of the surface and core Ag atoms, have been reported as standard techniques to produce exotic noble metal structures with hollow interiors, exhibiting unique physico-chemical properties.[35-37] Fig. 3A shows TEM and HRTEM images of the Au-based hollow nanostructures obtained by adding a specific amount of $HAuCl_4$ to an aqueous suspension of the Ag NRs in the presence of CTAB (see the ESI† for synthesis details). The use of CTAB as complexing agent assists the formation of Au complexes,[38] which controls the reactivity of the Au salt,[39] solubilizing at the same time the Ag insoluble species (AgCl) that are formed during the reaction.[35] As a result, highly crystalline AgAu hollow alloy nanostructures are obtained. Details of the indicated regions in Fig. 3A (FFT shown in inset and ESI† Fig S4) reveals the crystallinity of the obtained alloy structures, composed by a fcc AgAu phase.[35]

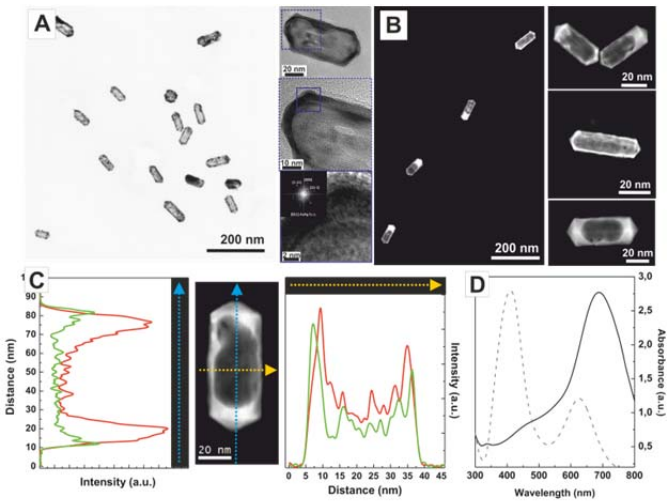

Fig. 3. A. TEM and HR-TEM images of AgAu hollow alloy NRs. Inset power spectra. B. HAADF STEM images of AgAu hollow alloy NRs. C. HAADF STEM images of a single AgAu hollow alloy NR and EDS line scan results through the blue (left) and yellow (right) arrow, where red line is Ag and green line is Au. D. UV-Vis absorption spectra of Ag NRs (grey-dotted line) and AgAu hollow alloy NRs (black line).

Fig. 3B shows HAADF-STEM images of the final hollow nanostructures where it can be clearly seen how they are faceted and retained the 5-twinned rod-like morphology of the original Ag NRs. Interestingly, despite the high uniformity, some of the obtained hollow structures present some inhomogeneities in terms of degree of voiding. This is associated to the limited range in GRR for mass transfer. Fig. 3C shows the STEM-EDS line scans obtained over the longitudinal (blue) and transverse (yellow) section of the hollow NRs. Elemental mapping profiles of Ag (red line) and Au (green line) indicate that end tips of the NR are mostly rich in Ag and covered by an outer thin (< 1nm) Au layer. Fig. 3D shows the UV-vis absorption spectra of a colloidal solution of as-synthesized NRs before (Ag NRs, dotted line), and after (Au hollow NRs, solid line), the addition of Au^{3+} precursor solution. Interestingly, the characteristic Ag absorption band at ~ 410 nm progressively vanishes while a new band at ~700 nm, corresponding to the SPR peak of the AgAu hollow NRs, gradually arises. Such hollow nanostructures strongly absorb in the water window (near Infrared) which opens their applicability in biomedical scenarios such as photo-thermally triggered drug release, optical imaging, and cancer phototherapy.[40]

In summary, we demonstrated a facile, robust and versatile approach to produce low aspect ratio Ag NRs in high yields. The method is based on the ethylene glycol reduction of CF_3COOAg in the presence of high molecular weight PVP, and tannic acid as co-reducing agent at sub-stoichiometric concentrations. In addition, we further demonstrated that the Ag NRs could be transformed into Au-based hollow nanostructures via the galvanic replacement reaction with $HAuCl_4$ at room temperature.

We acknowledge financial support from the Spanish Ministerio de Ciencia e Innovación (MICINN) (MAT2012-33330), the Catalan Agència de Gestió d'Ajuts Universitaris i de Recerca (AGAUR) (2014-SGR-612), QNano (INFRA-2010-262163), FutureNanoNeeds (FP7-NMP-2013-LARGE-7). N.G.B. acknowledges financial support by MINECO through the Ramon y Cajal program (RYC-2012- 10991) and by the European Commission Seventh Framework Programme (FP7) through the Marie Curie Career Integration Grant (322153-MINE).

Notes and references

1. M. Rycenga, C. M. Cobley, J. Zeng, W. Li, C. H. Moran, Q. Zhang, D. Qin and Y. Xia, *Chem. Rev.*, 2011, **111**, 3669.
2. B. Wiley, Y. Sun, B. Mayers and Y. Xia, *Chem. - Eur. J.*, 2005, **11**, 454.
3. N. R. Jana, L. Gearheart and C. J. Murphy, *Chem. Commun.*, 2001, DOI: 10.1039/b100521i, 617.
4. Q. Zhang and Y. Yin, *Chem. Commun.*, 2013, **49**, 215.
5. B. Pietrobon, M. McEachran and V. Kitaev, *ACS Nano*, 2009, **3**, 21.
6. J. Zhang, M. R. Langille and C. A. Mirkin, *Nano Lett.*, 2011, **11**, 2495.
7. J. Becker, I. Zins, A. Jakab, Y. Khalavka, O. Schubert and C. Sönnichsen, *Nano Lett.*, 2008, **8**, 1719.
8. D. Seo, C. I. Yoo, J. Jung and H. Song, *J. Am. Chem. Soc.*, 2008, **130**, 2940.
9. Y. Xiang, X. Wu, D. Liu, Z. Li, W. Chu, L. Feng, K. Zhang, W. Zhou and S. Xie, *Langmuir*, 2008, **24**, 3465.
10. R. Jiang, H. Chen, L. Shao, Q. Li and J. Wang, *Adv. Mater.*, 2012, **24**, OP200.
11. M. Luo, H. Huang, S.-I. Choi, C. Zhang, R. R. d. Silva, H.-C. Peng, Z.-Y. Li, J. Liu, Z. He and Y. Xia, *ACS Nano*, 2015, **9**, 10523.
12. W. Zhang, H. Y. J. Goh, S. Firdoz and X. Lu, *Chem. - Eur. J.*, 2013, **19**, 12732.
13. Y. Sun, B. Mayers, T. Herricks and Y. Xia, *Nano Lett.*, 2003, **3**, 955.
14. Y. Sun, Y. Yin, B. T. Mayers, T. Herricks and Y. Xia, *Chem. Mater.*, 2002, **14**, 4736.
15. Y. Sun, B. Gates, B. Mayers and Y. Xia, *Nano Lett.*, 2002, **2**, 165.
16. B. J. Wiley, S. H. Im, Z.-Y. Li, J. McLellan, A. Siekkinen and Y. Xia, *J. Phys. Chem. B*, 2006, **110**.
17. C. Chen, L. Wang, H. J. Yu, G. H. Jiang, Q. Yang, J. F. Zhou, W. D. Xiang and J. F. Zhang, *Mater. Chem. Phys.*, 2008, **107**, 13.
18. S. Guo, S. Dong and E. Wang, *Cryst Growth Des*, 2009, **9**, 372.
19. J. Jiu, K. Murai, D. Kim, K. Kim and K. Suganuma, *Mater. Chem. Phys.*, 2009, **114**, 333.
20. T. Maiyalagan, *Appl. Catal. A: General*, 2008, **340**, 191.
21. M. A. Mahmoud and M. A. El-Sayed, *The Journal of Physical Chemistry Letters*, 2013, **4**, 1541.
22. N. G. Bastús, F. Merkoçi, J. Piella and V. Puntes, *Chem. Mater.*, 2014, **26**, 2836.
23. J. Piella, N. G. Bastús and V. Puntes, *Chem. Mater.*, 2016, **28**, 1066.
24. S. I. Lim, M. Varon, I. Ojea-Jimenez, J. Arbiol and V. Puntes, *Chem. Mater.*, 2010, **22**, 4495.
25. S. I. Lim, I. Ojea-Jimenez, M. Varon, E. Casals, J. Arbiol and V. Puntes, *Nano Lett.*, 2010, **10**, 964.
26. N. G. Bastús, J. Comenge and V. F. Puntes, *Langmuir*, 2011, **27**, 11098.
27. H. Huang, L. Zhang, T. Lv, A. Ruditskiy, J. Liu, Z. Ye and Y. Xia, *ChemNanoMat*, 2015, **1**, 246.
28. W. A. Saidi, H. Feng and K. A. Fichthorn, *J. Phys. Chem. C*, 2013, **117**, 1163.
29. W. A. Al-Saidi, H. Feng and K. A. Fichthorn, *Nano Lett.*, 2012, **12**, 997.
30. X. Xia, J. Zeng, Q. Zhang, C. H. Moran and Y. Xia, *J. Phys. Chem. C*, 2012, **116**, 21647.
31. M. Tsuji, Y. Nishizawa, K. Matsumoto, M. Kubokawa, N. Miyamae and T. Tsuji, *Mater. Lett.*, 2006, **60**, 834.
32. A. Ruditskiy and Y. Xia, *J. Am. Chem. Soc.*, 2016, **138**, 3161.
33. Q. Zhang, W. Li, L.-P. Wen, J. Chen and Y. Xia, *Chem. - Eur. J.*, 2010, **16**, 10234.
34. X. Xia, Y. Wang, A. Ruditskiy and Y. Xia, *Adv. Mater.*, 2013, **25**, 6313.
35. E. González, J. Arbiol and V. F. Puntes, *Science*, 2011, **334**, 1377.
36. Y. Sun and Y. Xia, *Science*, 2002, **298**, 2176.
37. A. Genç, J. Patarroyo, J. Sancho-Parramon, R. Arenal, M. Duchamp, E. E. Gonzalez, L. Henrard, N. G. Bastús, R. E. Dunin-Borkowski, V. F. Puntes and J. Arbiol, *ACS Photonics*, 2016, **3**.
38. J. Rodríguez-Fernández, J. Pérez-Juste, P. Mulvaney and L. M. Liz-Marzán, *J. Phys. Chem. B*, 2005, **109**, 14257.
39. M. Varón, J. Arbiol and V. F. Puntes, *J. Phys. Chem. C*, 2015, **119**, 11818.
40. L. K. Bogart, G. Pourroy, C. J. Murphy, V. Puntes, T. Pellegrino, D. Rosenblum, D. Peer and R. Lévy, *ACS Nano*, 2014, **8**.

